

# Development of a data overflow protection system for Super-Kamiokande to maximize data from nearby supernovae

M. Mori<sup>19</sup>, K. Abe<sup>1,4</sup>, Y. Hayato<sup>1,4</sup>, K. Hiraide<sup>1,4</sup>, K. Hosokawa<sup>1,4</sup>, K. Ieki<sup>1,4</sup>,  
M. Ikeda<sup>1,4</sup>, J. Kameda<sup>1,4</sup>, Y. Kanemura<sup>1</sup>, R. Kaneshima<sup>1</sup>, Y. Kashiwagi<sup>1</sup>,  
Y. Kataoka<sup>1,4</sup>, S. Miki<sup>1</sup>, S. Mine<sup>1,8</sup>, M. Miura<sup>1,4</sup>, S. Moriyama<sup>1,4</sup>,  
Y. Nakano<sup>1</sup>, M. Nakahata<sup>1,4</sup>, S. Nakayama<sup>1,4</sup>, Y. Noguchi<sup>1</sup>, K. Okamoto<sup>1</sup>,  
K. Sato<sup>1</sup>, H. Sekiya<sup>1,4</sup>, H. Shiba<sup>1</sup>, K. Shimizu<sup>1</sup>, M. Shiozawa<sup>1,4</sup>, Y. Sonoda<sup>1</sup>,  
Y. Suzuki<sup>1</sup>, A. Takeda<sup>1,4</sup>, Y. Takemoto<sup>1,4</sup>, A. Takenaka<sup>1</sup>, H. Tanaka<sup>1,4</sup>,  
S. Watanabe<sup>1</sup>, T. Yano<sup>1</sup>, S. Han<sup>2</sup>, T. Kajita<sup>2,4,58</sup>, K. Okumura<sup>2,4</sup>,  
T. Tashiro<sup>2</sup>, T. Tomiya<sup>2</sup>, X. Wang<sup>2</sup>, S. Yoshida<sup>2</sup>, G. D. Megias<sup>3</sup>,  
P. Fernandez<sup>5</sup>, L. Labarga<sup>5</sup>, N. Ospina<sup>5</sup>, B. Zaldivar<sup>5</sup>, B. W. Pointon<sup>55,40</sup>,  
E. Kearns<sup>7,4</sup>, J. L. Raaf<sup>7</sup>, L. Wan<sup>7</sup>, T. Wester<sup>7</sup>, J. Bian<sup>8</sup>, N. J. Griskevich<sup>8</sup>,  
S. Locke<sup>8</sup>, M. B. Smy<sup>8,4</sup>, H. W. Sobel<sup>8,4</sup>, V. Takhistov<sup>8,17</sup>, A. Yankelevich<sup>8</sup>,  
J. Hill<sup>9</sup>, M. C. Jang<sup>10</sup>, S. H. Lee<sup>10</sup>, D. H. Moon<sup>10</sup>, R. G. Park<sup>10</sup>, B. Bodur<sup>11</sup>,  
K. Scholberg<sup>11</sup>, C. W. Walter<sup>11,4</sup>, A. Beauchêne<sup>44</sup>, O. Drapier<sup>44</sup>,  
A. Giampaolo<sup>44</sup>, Th. A. Mueller<sup>44</sup>, A. D. Santos<sup>44</sup>, P. Paganini<sup>44</sup>,  
B. Quilain<sup>44</sup>, R. Rogly<sup>44</sup>, T. Ishizuka<sup>12</sup>, T. Nakamura<sup>13</sup>, J. S. Jang<sup>14</sup>,  
J. G. Learned<sup>15</sup>, K. Choi<sup>59</sup>, N. Iovine<sup>59</sup>, S. Cao<sup>57</sup>, L. H. V. Anthony<sup>16</sup>,  
D. Martin<sup>16</sup>, M. Scott<sup>16</sup>, A. A. Sztuc<sup>16</sup>, Y. Uchida<sup>16</sup>, V. Berardi<sup>45</sup>,  
M. G. Catanesi<sup>45</sup>, E. Radicioni<sup>45</sup>, N. F. Calabria<sup>46</sup>, A. Langella<sup>46</sup>,  
L. N. Machado<sup>46</sup>, G. De Rosa<sup>46</sup>, G. Collazuol<sup>48</sup>, F. Iacob<sup>48</sup>,  
M. Lamoureux<sup>48</sup>, M. Mattiazzi<sup>48</sup>, L. Ludovici<sup>47</sup>, M. Gonin<sup>58</sup>, L. Perisse<sup>58</sup>,  
G. Pronost<sup>58</sup>, C. Fujisawa<sup>49</sup>, Y. Maekawa<sup>49</sup>, Y. Nishimura<sup>49</sup>, R. Okazaki<sup>49</sup>,  
R. Akutsu<sup>17</sup>, M. Friend<sup>17</sup>, T. Hasegawa<sup>17</sup>, T. Ishida<sup>17</sup>, T. Kobayashi<sup>17</sup>,  
M. Jakkapu<sup>17</sup>, T. Matsubara<sup>17</sup>, T. Nakadaira<sup>17</sup>, K. Nakamura<sup>17,4</sup>,  
Y. Oyama<sup>17</sup>, K. Sakashita<sup>17</sup>, T. Sekiguchi<sup>17</sup>, T. Tsukamoto<sup>17</sup>, N. Bhuiyan<sup>51</sup>,

G. T. Burton<sup>51</sup>, R. Edwards<sup>51</sup>, F. Di Lodovico<sup>51</sup>, J. Gao<sup>51</sup>, A. Goldsack<sup>51</sup>,  
 T. Katori<sup>51</sup>, J. Migenda<sup>51</sup>, R. M. Ramsden<sup>51</sup>, Z. Xie<sup>51</sup>, S. Zsoldos<sup>51,4</sup>,  
 Y. Kotsar<sup>18</sup>, H. Ozaki<sup>18</sup>, A. T. Suzuki<sup>18</sup>, Y. Takagi<sup>18</sup>, Y. Takeuchi<sup>18,4</sup>,  
 H. Zhong<sup>18</sup>, C. Bronner<sup>19</sup>, J. Feng<sup>19</sup>, J. R. Hu<sup>19</sup>, Z. Hu<sup>19</sup>, M. Kawaune<sup>19</sup>,  
 T. Kikawa<sup>19</sup>, F. LiCheng<sup>19</sup>, T. Nakaya<sup>19,4</sup>, R. A. Wendell<sup>19,4</sup>, K. Yasutome<sup>19</sup>,  
 S. J. Jenkins<sup>20</sup>, N. McCauley<sup>20</sup>, P. Mehta<sup>20</sup>, A. Tarant<sup>20</sup>, Y. Fukuda<sup>21</sup>,  
 Y. Itow<sup>22,23</sup>, H. Menjo<sup>22</sup>, K. Ninomiya<sup>22</sup>, Y. Yoshioka<sup>22</sup>, J. Lagoda<sup>24</sup>,  
 S. M. Lakshmi<sup>24</sup>, M. Mandal<sup>24</sup>, P. Mijakowski<sup>24</sup>, Y. S. Prabhu<sup>24</sup>,  
 J. Zalipska<sup>24</sup>, M. Jia<sup>25</sup>, J. Jiang<sup>25</sup>, C. K. Jung<sup>25</sup>, W. Shi<sup>25</sup>, M. J. Wilking<sup>25</sup>,  
 C. Yanagisawa<sup>25†</sup>, M. Harada<sup>26</sup>, Y. Hino<sup>26</sup>, H. Ishino<sup>26</sup>, H. Kitagawa<sup>26</sup>,  
 Y. Koshio<sup>26,4</sup>, F. Nakanishi<sup>26</sup>, S. Sakai<sup>26</sup>, T. Tada<sup>26</sup>, T. Tano<sup>26</sup>, G. Barr<sup>28</sup>,  
 D. Barrow<sup>28</sup>, L. Cook<sup>28,4</sup>, S. Samani<sup>28</sup>, D. Wark<sup>28,34</sup>, A. Holin<sup>53</sup>, F. Nova<sup>53</sup>,  
 S. Jung<sup>31</sup>, B. S. Yang<sup>31</sup>, J. Y. Yang<sup>31</sup>, J. Yoo<sup>31</sup>, J. E. P. Fannon<sup>32</sup>,  
 L. Kneale<sup>32</sup>, M. Malek<sup>32</sup>, J. M. McElwee<sup>32</sup>, M. D. Thiesse<sup>32</sup>,  
 L. F. Thompson<sup>32</sup>, S. Wilson<sup>32</sup>, H. Okazawa<sup>33</sup>, S. B. Kim<sup>35</sup>, E. Kwon<sup>35</sup>,  
 J. W. Seo<sup>35</sup>, I. Yu<sup>35</sup>, A. K. Ichikawa<sup>56</sup>, K. D. Nakamura<sup>56</sup>, S. Tairafune<sup>56</sup>,  
 K. Nishijima<sup>41</sup>, A. Eguchi<sup>36</sup>, K. Nakagiri<sup>36</sup>, Y. Nakajima<sup>36,4</sup>, S. Shima<sup>36</sup>,  
 N. Taniuchi<sup>36</sup>, E. Watanabe<sup>36</sup>, M. Yokoyama<sup>36,4</sup>, P. de Perio<sup>4</sup>, S. Fujita<sup>4</sup>,  
 K. Martens<sup>4</sup>, K. M. Tsui<sup>4</sup>, M. R. Vagins<sup>4,8</sup>, C. J. Valls<sup>4,36</sup>, J. Xia<sup>4</sup>,  
 M. Kuze<sup>37</sup>, S. Izumiyama<sup>37</sup>, M. Ishitsuka<sup>38</sup>, H. Ito<sup>38</sup>, T. Kinoshita<sup>38</sup>,  
 R. Matsumoto<sup>38</sup>, Y. Ommura<sup>38</sup>, N. Shigeta<sup>38</sup>, M. Shinoki<sup>38</sup>, T. Suganuma<sup>38</sup>,  
 K. Yamauchi<sup>38</sup>, T. Yoshida<sup>38</sup>, J. F. Martin<sup>39</sup>, H. A. Tanaka<sup>39</sup>,  
 T. Towstego<sup>39</sup>, R. Gaur<sup>40</sup>, V. Gousy-Leblanc<sup>40‡</sup>, M. Hartz<sup>40</sup>, A. Konaka<sup>40</sup>,  
 X. Li<sup>40</sup>, N. W. Prouse<sup>40</sup>, S. Chen<sup>42</sup>, B. D. Xu<sup>42</sup>, B. Zhang<sup>42</sup>,  
 M. Posiadala-Zezula<sup>54</sup>, S. B. Boyd<sup>52</sup>, D. Hadley<sup>52</sup>, M. Nicholson<sup>52</sup>,  
 M. O’Flaherty<sup>52</sup>, B. Richards<sup>52</sup>, A. Ali<sup>50,40</sup>, B. Jamieson<sup>50</sup>, S. Amanai<sup>43</sup>,  
 Ll. Marti<sup>43</sup>, A. Minamino<sup>43</sup>, G. Pintaudi<sup>43</sup>, S. Sano<sup>43</sup>, S. Suzuki<sup>43</sup>,  
 K. Wada<sup>43</sup>, **(The Super-Kamiokande Collaboration)**

<sup>1</sup>*Kamioka Observatory, Institute for Cosmic Ray Research, University of Tokyo, Kamioka, Gifu 506-1205, Japan*

<sup>2</sup>*Research Center for Cosmic Neutrinos, Institute for Cosmic Ray Research, University of Tokyo, Kashiwa, Chiba 277-8582, Japan*

<sup>3</sup>*Institute for Cosmic Ray Research, University of Tokyo, Kashiwa, Chiba 277-8582, Japan*

<sup>4</sup>*Kavli Institute for the Physics and Mathematics of the Universe (WPI), The University of Tokyo Institutes for Advanced Study, University of Tokyo, Kashiwa, Chiba 277-8583, Japan*

<sup>5</sup>*Department of Theoretical Physics, University Autonoma Madrid, 28049 Madrid, Spain*

<sup>6</sup>*Department of Physics and Astronomy, University of British Columbia, Vancouver, BC, V6T1Z4, Canada*

<sup>7</sup>*Department of Physics, Boston University, Boston, MA 02215, USA*

<sup>8</sup>*Department of Physics and Astronomy, University of California, Irvine, Irvine, CA 92697-4575, USA*

<sup>9</sup>*Department of Physics, California State University, Dominguez Hills, Carson, CA 90747, USA*

<sup>10</sup>*Institute for Universe and Elementary Particles, Chonnam National University, Gwangju 61186, Korea*

<sup>11</sup>*Department of Physics, Duke University, Durham NC 27708, USA*

<sup>12</sup>*Junior College, Fukuoka Institute of Technology, Fukuoka, Fukuoka 811-0295, Japan*

<sup>13</sup>*Department of Physics, Gifu University, Gifu, Gifu 501-1193, Japan*

<sup>14</sup>*GIST College, Gwangju Institute of Science and Technology, Gwangju 500-712, Korea*

<sup>15</sup>*Department of Physics and Astronomy, University of Hawaii, Honolulu, HI 96822, USA*

- <sup>16</sup>*Department of Physics, Imperial College London , London, SW7 2AZ,  
United Kingdom*
- <sup>17</sup>*High Energy Accelerator Research Organization (KEK), Tsukuba, Ibaraki  
305-0801, Japan*
- <sup>18</sup>*Department of Physics, Kobe University, Kobe, Hyogo 657-8501, Japan*
- <sup>19</sup>*Department of Physics, Kyoto University, Kyoto, Kyoto 606-8502, Japan*
- <sup>20</sup>*Department of Physics, University of Liverpool, Liverpool, L69 7ZE,  
United Kingdom*
- <sup>21</sup>*Department of Physics, Miyagi University of Education, Sendai, Miyagi  
980-0845, Japan*
- <sup>22</sup>*Institute for Space-Earth Environmental Research, Nagoya University,  
Nagoya, Aichi 464-8602, Japan*
- <sup>23</sup>*Kobayashi-Maskawa Institute for the Origin of Particles and the Universe,  
Nagoya University, Nagoya, Aichi 464-8602, Japan*
- <sup>24</sup>*National Centre For Nuclear Research, 02-093 Warsaw, Poland*
- <sup>25</sup>*Department of Physics and Astronomy, State University of New York at  
Stony Brook, NY 11794-3800, USA*
- <sup>26</sup>*Department of Physics, Okayama University, Okayama, Okayama  
700-8530, Japan*
- <sup>27</sup>*Department of Physics, Osaka University, Toyonaka, Osaka 560-0043,  
Japan*
- <sup>28</sup>*Department of Physics, Oxford University, Oxford, OX1 3PU, United  
Kingdom*
- <sup>29</sup>*School of Physics and Astronomy, Queen Mary University of London,  
London, E1 4NS, United Kingdom*
- <sup>30</sup>*Department of Physics, University of Regina, 3737 Wascana Parkway,  
Regina, SK, S4S0A2, Canada*
- <sup>31</sup>*Department of Physics, Seoul National University, Seoul 151-742, Korea*

- <sup>32</sup>*Department of Physics and Astronomy, University of Sheffield, S3 7RH,  
Sheffield, United Kingdom*
- <sup>33</sup>*Department of Informatics in Social Welfare, Shizuoka University of  
Welfare, Yaizu, Shizuoka, 425-8611, Japan*
- <sup>34</sup>*STFC, Rutherford Appleton Laboratory, Harwell Oxford, and Daresbury  
Laboratory, Warrington, OX11 0QX, United Kingdom*
- <sup>35</sup>*Department of Physics, Sungkyunkwan University, Suwon 440-746, Korea*
- <sup>36</sup>*Department of Physics, University of Tokyo, Bunkyo, Tokyo 113-0033,  
Japan*
- <sup>37</sup>*Department of Physics, Tokyo Institute of Technology, Meguro, Tokyo  
152-8551, Japan*
- <sup>38</sup>*Department of Physics, Faculty of Science and Technology, Tokyo  
University of Science, Noda, Chiba 278-8510, Japan*
- <sup>39</sup>*Department of Physics, University of Toronto, ON, M5S 1A7, Canada*
- <sup>40</sup>*TRIUMF, 4004 Wesbrook Mall, Vancouver, BC, V6T2A3, Canada*
- <sup>41</sup>*Department of Physics, Tokai University, Hiratsuka, Kanagawa 259-1292,  
Japan*
- <sup>42</sup>*Department of Engineering Physics, Tsinghua University, Beijing,  
100084, China*
- <sup>43</sup>*Department of Physics, Yokohama National University, Yokohama,  
Kanagawa, 240-8501, Japan*
- <sup>44</sup>*Ecole Polytechnique, IN2P3-CNRS, Laboratoire Leprince-Ringuet,  
F-91120 Palaiseau, France*
- <sup>45</sup>*Dipartimento Interuniversitario di Fisica, INFN Sezione di Bari and  
Università e Politecnico di Bari, I-70125, Bari, Italy*
- <sup>46</sup>*Dipartimento di Fisica, INFN Sezione di Napoli and Università di Napoli,  
I-80126, Napoli, Italy*
- <sup>47</sup>*INFN Sezione di Roma and Università di Roma “La Sapienza”, I-00185,  
Roma, Italy*

<sup>48</sup>*Dipartimento di Fisica, INFN Sezione di Padova and Università di  
Padova, I-35131, Padova, Italy*

<sup>49</sup>*Department of Physics, Keio University, Yokohama, Kanagawa, 223-8522,  
Japan*

<sup>50</sup>*Department of Physics, University of Winnipeg, MB R3J 3L8, Canada*

<sup>51</sup>*Department of Physics, King's College London, London, WC2R 2LS, UK*

<sup>52</sup>*Department of Physics, University of Warwick, Coventry, CV4 7AL, UK*

<sup>53</sup>*Rutherford Appleton Laboratory, Harwell, Oxford, OX11 0QX, UK*

<sup>54</sup>*Faculty of Physics, University of Warsaw, Warsaw, 02-093, Poland*

<sup>55</sup>*Department of Physics, British Columbia Institute of Technology,  
Burnaby, BC, V5G 3H2, Canada*

<sup>56</sup>*Department of Physics, Faculty of Science, Tohoku University, Sendai,  
Miyagi, 980-8578, Japan*

<sup>57</sup>*Institute For Interdisciplinary Research in Science and Education, ICISE,  
Quy Nhon, 55121, Vietnam*

<sup>58</sup>*ILANCE, CNRS - University of Tokyo International Research Laboratory,  
Kashiwa, Chiba 277-8582, Japan*

<sup>59</sup>*Institute for Basic Science (IBS), Daejeon, 34126, Korea*

.....  
Neutrinos from very nearby supernovae, such as Betelgeuse, are expected to generate more than ten million events over 10s in Super-Kamokande (SK). At such large event rates, the buffers of the SK analog-to-digital conversion board (QBEE) will overflow, causing random loss of data that is critical for understanding the dynamics of the supernova explosion mechanism. In order to solve this problem, two new DAQ modules were developed to aid in the observation of very nearby supernovae. The first of these, the SN module, is designed to save only the number of hit PMTs during a supernova burst and the second, the Veto module, prescales the high rate neutrino events to prevent the QBEE from overflowing based on information from the SN module. In the event of a very nearby supernova, these modules allow SK to reconstruct the time evolution of the neutrino event rate from beginning to end using both QBEE and SN module data. This paper presents the development and testing of these modules together with an analysis of supernova-like data generated with a flashing laser diode. We demonstrate that the Veto module successfully prevents DAQ overflows for Betelgeuse-like supernovae as well as the long-term stability of the new modules. During normal running the Veto module is found to issue DAQ vetos a few times per month resulting in a total dead time less than 1 ms, and does not influence ordinary operations. Additionally, using simulation data we find that supernovae closer than 800 pc will trigger Veto module resulting in a prescaling of the observed neutrino data.  
.....

---

<sup>†</sup> also at BMCC/CUNY, Science Department, New York, New York, 1007, USA.  
<sup>‡</sup> also at University of Victoria, Department of Physics and Astronomy, PO Box 1700 STN CSC, Victoria,  
BC V8W 2Y2, Canada.

# 1 Introduction

Core-collapse Supernovae (CCSNe) are one of the most energetic explosions in the universe. The release of gravitational energy reaches about  $10^{53}$  erg and more than 90% of that energy is thought to be released as neutrinos [1–3]. After the explosion supernovae leave behind compact objects, neutron stars or black holes. Due to extremely dense matter at the core of the supernova observation of star’s interior during the explosion via electromagnetic signals is difficult, making it harder to understand the formation of those compact objects. However, since neutrinos rarely interact with matter they can carry information about the inner cores of the exploding star, such that their observation on Earth allows for the study of the explosion mechanism, the structure of neutron star, and the formation of black holes. For this reason neutrino detectors all over the world are preparing to observe events from the next galactic supernova.

Super-Kamiokande (SK) [4] is a water Cherenkov detector located about 1000 m under Mt. Ikeno in Gifu prefecture, Japan, and is continually monitoring for supernova neutrinos. SK is composed of a stainless steel tank filled with of 50.0 kton ultrapure water. The tank is optically separated into two regions: an inner detector (ID) and an outer detector (OD). The 32.5 kton ID is equipped with 11,129 inward-facing 20-inch photomultiplier tubes (PMTs) to observe Cherenkov rings formed by charged particles traversing its interior. To identify incoming particles, such as cosmic ray muons, and to tag particles going out from the ID, the OD is instrumented with 1,885 outward-facing 8-inch PMTs coupled to wavelength-shifting plates. Although typical SK analyses use an ID fiducial volume of 22.5 kton to 27.2 kton, the full volume of the ID is expected to be useable during supernova neutrino bursts [5].

Based on the observations of neutrinos from SN 1987A [6–8], humanity’s only detection of a CCSN via neutrinos so far, thousands of neutrino events are expected to be detected with SK [9] for a galactic CCSN. For a closer SN, such as Betelgeuse, over tens of thousands of events are expected within a minute. Indeed, we consider the observation of Betelgeuse with the SK. Given that the Kamiokande experiment observed 11 events from SN 1987A which is located in the LMC at 51.2 kpc, and the distance to Betelgeuse is  $168_{-15}^{+28}$  pc [10], we anticipate that  $11\text{M} - 20\text{M}$  events interactions will occur over 10 seconds within the ID full volume of SK. This number of events is too many for the current SK data-acquisition (DAQ) system to process. Accordingly, we have developed new DAQ modules specifically to enable recording of events from a very nearby supernova to address this problem. Two modules have been newly developed, one of which records only the PMT hit rate before any time and charge information is extracted from the standard DAQ and another that prescales the data



passed to that DAQ when the event rate becomes large. The development and performance of these modules is discussed below.

## 2 Current SK DAQ

Prior to 2008 so-called Analog Timing Modules(ATMs) were used to digitize the analog PMT signals in SK following a hardware-based trigger decision. The ATM suffered dead time as a result of its slow digital conversion time as well as slow data processing and readout speeds. During the conversion and readout, only a maximum of subsequently triggered 2 events could be recorded. To overcome these limitations, the SK front-end electronics were replaced with the QTC Based Electronics with Ethernet (QBEE) module, which continuously records all PMT hits in the detector, including dark noise and other spurious signals, and sends the data to a software-based trigger system. The QBEE-based DAQ system realizes dead-time-free data taking at lower energy thresholds than the ATM system. Further, while the ATM is capable of processing a trigger rate up to 4 kHz, roughly the rate expected from a CCSN at 5 kpc, the QBEE can handle more than 20 kHz.

Figure 1 shows the nominal data flow in SK since 2008. In total there are 550 QBEE boards each of which is connected to up to 24 PMTs and is stored in one of four huts at the top of the SK tank. These huts divide the detector into quadrants and also hold house HV power supplies for the PMTs as well as front-end readout computers. Each QBEE has eight charge-to-time converters (QTC) [11] and four time-to-digital converters (TDC (AMT (Atlas Muon TDC))) [12] for digitization. When relativistic charged particles traverse the SK tank the emitted Cherenkov light is converted to analog electrical pulses by the PMTs. These analog pulses are converted to digital signals via the QBEE's onboard QTC before being processed with the TDC. After this step twelve readout computers collate the data from the entire detector into time series before passing them to eight computers dedicated to apply the software-based trigger to form events. Triggered events are stored to disk after removing PMT hits occurring in multiple events.

All QBEEs are synchronized by a master-clock module (MCM) capable of distributing a 60 MHz and 60 kHz clock. The 60 kHz clock signal is passed to an event-counting module (TRG32), which passes the generated event count (termed "hardware counter" elsewhere in this paper) back to the MCM for redistribution to the QBEEs. The 60 kHz clock is also used to reset the QBEE TDC thereby synchronizing the PMTs to the MCM clock. We note that a pedestal trigger is also generated using the 60 kHz clock of the MCM.

In order to identify interesting regions in the data stream, the software trigger utilizes the number of PMT hits in a sliding 200 ns time window to make trigger decisions. The criteria for

various triggers are summarized in Table 1. Currently the DAQ system provides essentially dead-time free acquisition of all PMT hits above these thresholds. Supernova neutrinos are expected to generate primarily SLE, LE and HE triggered events. For electrons with kinetic energies greater than 3.5 MeV the SLE trigger efficiency is 100%, whereas above 5.4 MeV (8.5 MeV), the LE trigger efficiency is 50% (100%). Both efficiencies include the impact of the few kHz dark noise generated by the ID PMTs.

Trigger Types	Criteria	Time Windows[ $\mu$ s]
SLE	$N_{200} > 31$	[-1.5, +1.0]
LE	$N_{200} > 47$	[-5,+35]
HE	$N_{200} > 50$	[-5,+35]
SHE	$N_{200} > 58$	[-5,+35]
OD	$N_{200} > 22$ in OD	[-5,+35]
AFT	SHE + no OD	[+35,+535]

**Table 1** Summary of the SK event trigger menu, where  $N_{200}$  is the number of PMT hits in a sliding 200 ns time window. Here OD refers to the number of hit PMTs in the outer detector. These conditions are current as of 2023 and may vary according to the situation of the detector, for example, dark rate.

### 2.1 Limitations of the current system

While the QBEE can handle higher event rates than the previous ATM module, for extremely large data rates, such as those expected from a nearby supernova, buffers on the board as well as downstream DAQ computers may overflow resulting in a loss data. Figure 2 shows a simplified block diagram of the QBEE board. Each QBEE is connected to PMTs via the PMT interface and has three circuits to measure the observed charge over separate ranges in order to keep linearity. Analog pulses from the PMTs are converted by the QTC into rectangular pulses whose widths correspond to the total charge in the input signal. These rectangular pulses are then converted to digital signals by the TDC. A field programmable array (FPGA) located downstream of the TDC then converts the width between the rise and fall of a pulse into charge, divides the data into blocks of hardware counters and chooses a suitable charge integration range for the signal. Finally, the digitized data are transmitted to the readout computer through the daughter board (DB).

The QBEE board is equipped with three types of memory to store pulse information: TDC memory (L1 buffer), FIFO memory and a buffer on the daughter board. The L1 buffer is

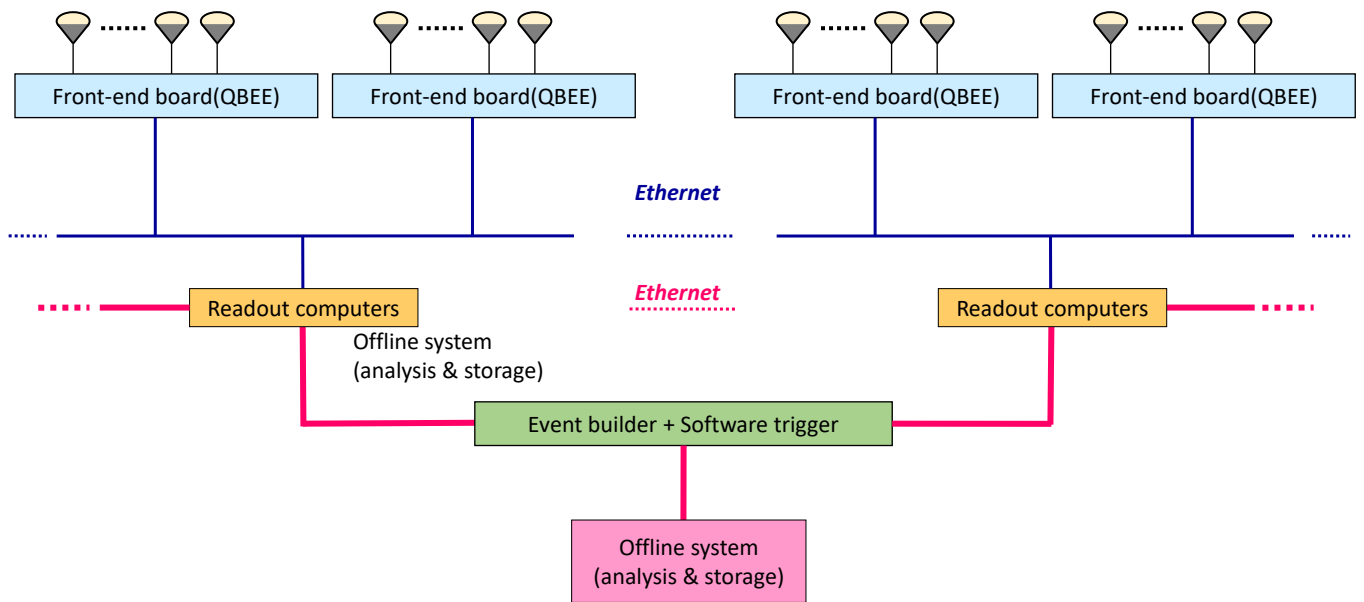


**Fig. 1** Schematic diagram of the flow of data in the SK DAQ system.

used to store pulses within the TDC and it is the smallest of the three. Pulses being processed by the FPGA are stored in the FIFO memory and the onboard DB buffer stores data before being sent to the readout computers. Under normal run conditions these buffer memories do not overflow, though it can happen in the L1 buffer following very high charge signals from energetic through going muons, that induce multiple rapid pulses in the PMTs. However, a supernova such as Betelgeuse, which is predicted to generate tens to thirty million events over 10 seconds, can cause overflow in these buffers. When the buffers are full additional data is discarded, resulting in a loss of information available to reconstruct individual events.

### 3 New modules for overflow protection

To overcome the difficulties described above, two new DAQ modules have been developed, the SN module [13] and the Veto module. Conceptually the Veto module serves to limit the amount of data that the QBEE processes during a very near supernova burst, taking as input the PMT hit rate recorded by the SN module. The SN module records the PMT hit rate without incurring any dead time. Indeed, the hit rate serves as a proxy for the rate of energy deposition and even by itself is useful in the analysis of supernova data. These two modules make it possible for dead-time free data acquisition and for the prevention

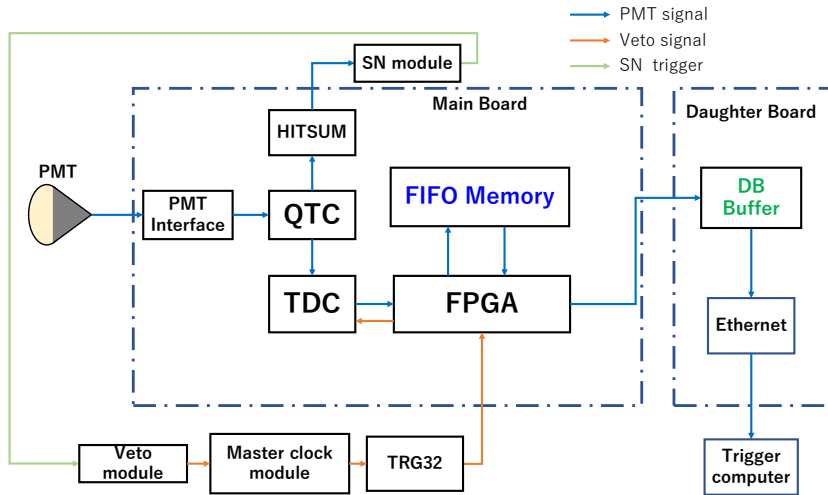


**Fig. 2** Simplified Block diagram of the QBEE.

of uncontrolled data loss caused by QBEE memory overflows. As explained below the SN module records only the number of hit PMTs continuously and is not subject to memory overflow issues. When the Veto module detects a PMT hit rate that is too high for the QBEE, it issues a veto to stop QBEE processing, thereby prescaling the event rate it sees. During this veto the QBEE does not store data. However, for the low energies typical of neutrinos from supernovae, the number of hit PMTs is proportional to the neutrino energy so the loss of QBEE data is compensated by the number of hit PMTs stored by the SN module.

In order to extract the most information from a supernova burst in which the QBEE is periodically vetoed in this way, we must rely on the PMT hitsum provided by the SN module and supplemental information from the QBEEs during periods where no veto is issued. Assuming that the distribution of neutrino energies does not change appreciably during the veto window, typically  $17 \mu s$ , the flux of neutrinos during that time can be extracted from the QBEE information recorded during the surrounding non-vetoed time periods. In short, the QBEE's measurements of the number of PMT hits taken together with reconstructed event energies can be used to extract the flux given the PMT HITSUM provided by the SN module during the veto period.

### 3.1 SN module

The SN module is a dedicated system that records the total number of PMT hits (HITSUM) in the detector [13]. This HITSUM is calculated by the QBEE, but importantly is done upstream of the QBEE memory storage as shown in Figure 2. For this reason the HITSUM

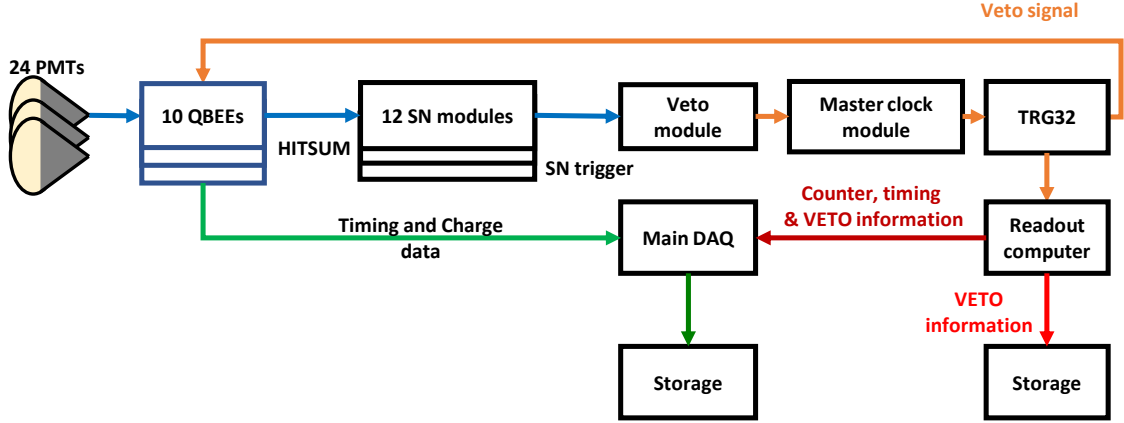


**Fig. 3** Relationship between the QBEE, SN module and Veto module as well as the flow of their data.

calculation operates independently of the TDC and is not affected by memory overflows when the hit rate becomes large. The SN module reads out the HITSUM at 60 MHz from the circuit, sums up those hits at 60 kHz and saves it together with the hardware counter associated to those hits.

Each of SK’s electronics huts houses 12 SN modules and each board is attached to 10 QBEEs (Figure 3). The SN module issues a trigger when the HITSUM exceeds a programmable threshold. Currently one SN module will issue a trigger when there are more than 100 PMT hits in each of four consecutive hardware counters, roughly  $68 \mu\text{s}$ . The Veto module, described later, uses the number of SN module boards issues triggers to determine when the QBEEs should be vetoed.

### 3.2 Veto module

The Veto module is designed to prescale the number of PMT hits to prevent the QBEEs from overflowing. The Veto module was officially put into operation in June 2021. Each Veto module is connected to 12 SN modules such that its veto decision is based on the activity of PMTs in each quadrant of the detector. For a nearby supernova the rapid succession of neutrino interactions in the detector is expected to produce a burst of PMT hit activity that will trigger the SN modules. Looking at those SN module triggers the Veto module vetos

Threshold of SN trigger	Length of continuous excessive SN trigger	Prescaling rate
8	4	1/4
10	100	1/5
10	1000	1/6

**Table 2** Trigger conditions for issuing a veto with the Veto module.

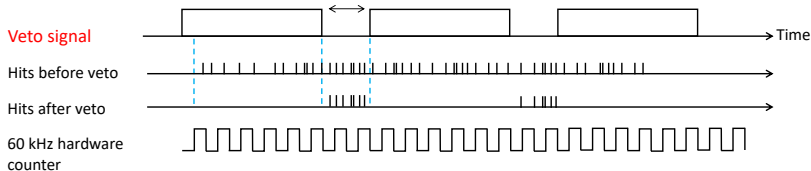


**Fig. 4** Time structure of the veto signal to implement a 1/4 prescale factor.

QBEE activity at and downstream of the TDC to prevent memory overflows. Table 2 lists the conditions under which the module issues a veto together with the corresponding prescale rates. These conditions were determined with laser diode test data as described in the next section. Figure 4 shows the timing diagram issued veto signals. Based on the activity in the detector the veto may be applied over several hardware counters, but when the veto is lifted there will be at least two hardware contours before another veto is possible. Note that the Veto module runs with an internal clock and is not synchronized with the QBEEs.

When the event rate triggers the Veto module, a veto signal is first sent to the master clock module (Figure 2) whose primary function is to distribute clock signals and hardware counters to all QBEE boards. Upon receipt of a signal from the Veto module though, the master clock module then distributes the veto signal to all QBEEs using the next clock. Veto signals are transmitted to the TDC on QBEE, stopping its function. As a result, the TDC discards any received pulses during one  $17 \mu\text{s}$  cycle while the veto is applied. Note that the veto signals do not have any influence on HITSUM, which continues to process PMT hits since it is independent of the TDC. Veto signals are recorded via the TRG32 in Figure 3 independently of the main DAQ so that we exactly know when veto signals issue even if the QBEEs stop due to an overflow or due to the veto signals themselves.

## 4 Performance tests of the new modules

The performance of the SN modules and Veto modules was evaluated using dedicated data designed to simulate the event rate expected during a nearby supernova. These tests

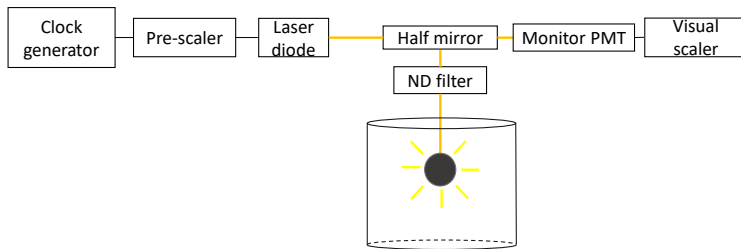


**Fig. 5** Setup of the LD test.

confirmed that the data are sufficiently prescaled to prevent memory overflows and further that they have no influence on normal observation periods.

#### 4.1 Laser Diode testing

A laser diode (LD) connected to a diffuser ball located near the center of the SK tank is used to approximately reproduce the expected event rate of a supernova. For the tests described in this subsection we modified the total event rate of the simulated supernovae, while keeping the timing structure constant, to probe the limitations of the main DAQ without the benefit of the new modules.

Figure 5 shows the setup of the LD test. Light from the LD is isotropically emitted from the diffuser ball with the time structure shown in Figure 6. A flash roughly generates 130 PMT hits, which correspond to 6 MeV. The time structure has been chosen to mimic that predicted by supernova models: the first 0.5s corresponds to the sharp increase in the event rate expected from the neutronization burst, which decays rapidly over one second before the event rate gently slows for up to 10s during the neutron star cooling phase. Setting the LD system to produce 60 million events over the 10s burst is a sufficient test of the DAQ system as it exceeds the event rate expected from Betelgeuse (10–30 million events, depending upon the model).

#### 4.2 LD tests with and without the Veto module

Without employing the Veto module and setting the total number of LD-generated events to 30 million results in the QBEE data shown in Figure 7. The vertical axis shows the number of hit PMTs per hardware counter ( $17 \mu s$ ) and the blue and green markers show the number of boards in which FIFO overflow and DB overflow occurs, respectively. Comparing Figure 7 and Figure 6, it is clear that the simulated burst structure is significantly affected during periods of overflow.

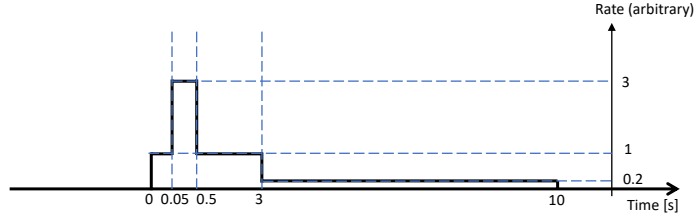


**Fig. 6** Time structure of the LD burst. Changing the total number of flashes, does not affect the horizontal time structure but instead increases the number of events in each section.

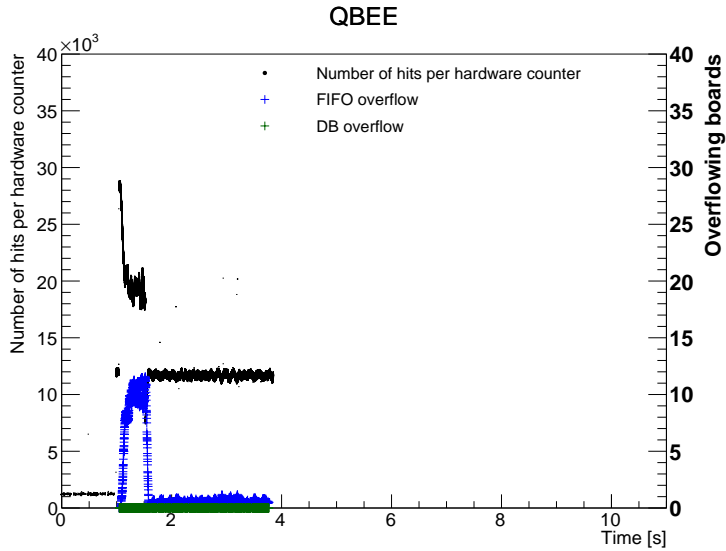


**Fig. 7** An LD test with 30 million burst events recorded with the QBEE. The black dots are the number of LD flashes per hardware counter ( $\approx 17.1 \mu\text{s}$ ). Blue markers represent the number QBEE boards per hardware counter of which experience a FIFO buffer overflow. Green points show overflow for the daughterboard. The burst structure is disturbed by the overflow of the QBEE. In this case, SK failed to record correct data after 4 s of this data.

Connecting the Veto module and repeating the test results in data shown in Figure 8. Comparing again Figure 7 and Figure 8, we note that the Veto module completely prevents the QBEE from overflowing. Further, the time structure of the LD data is completely retained following closely the original (Figure 6). There is a zero hit cluster from 1 s to 1.5 s. The time is the highest rate time Figure 9 shows the same data set as recorded by the SN module.



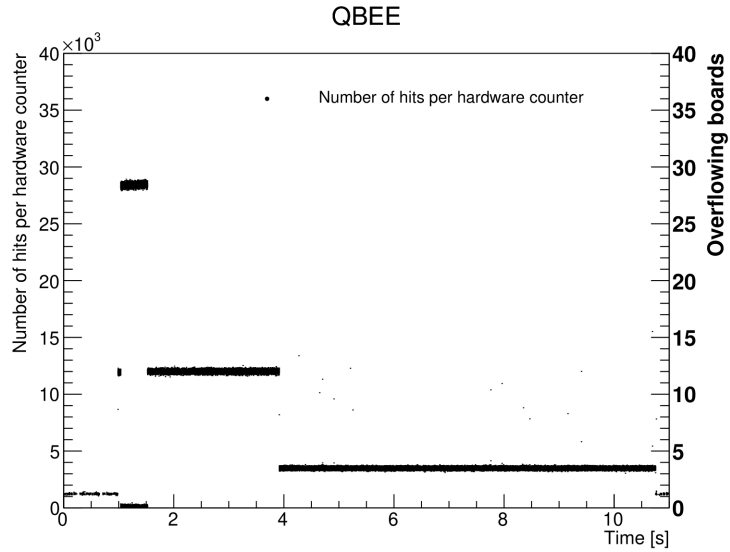


**Fig. 8** An LD burst test with 30 million events when the QBEE is connected to the Veto module. Here the burst shape is not disturbed. The cluster of zero hit from 1 s to 1.5 s is due to the Veto module. There is no QBEE overflow during the burst.

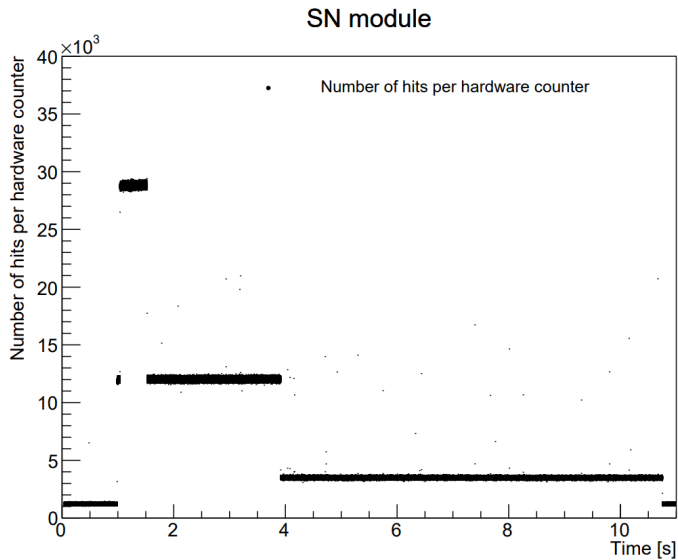


**Fig. 9** An LD burst test with 30 million events as recorded by the SN module. Note that this module can record the entirety of the LD burst.

It is unaffected by the Veto module, as expected. Note that the baseline heights in the SN and QBEE data are different because the latter records only triggered events, whereas the former continuously records all PMT hits.

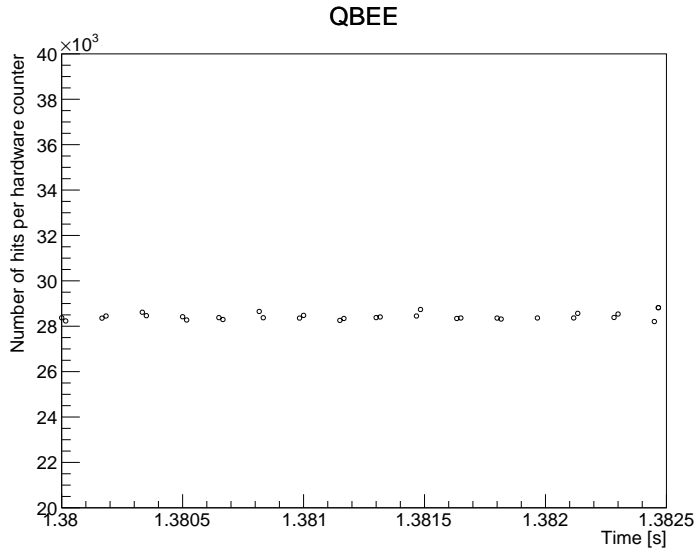


**Fig. 10** Zoom in of Figure 8 showing the structure of the veto signal. The veto length is 6 counters ( $103 \mu\text{s}$ ) and the veto break length is 2 counters ( $34.1 \mu\text{s}$ ). Paired dots are recorded PMT hits. There is an isolated dot at 1.382s due to a mismatch between the QBEE and Veto module clock signals.

### 4.3 Recorded hits from LD bursts

Here we consider the results of four LD burst tests and compare their total number of hit PMTs. Defining the onset of a burst as the time when the number of hits in  $17.1 \mu\text{s}$  exceeds 10,000 consistently for  $170.7 \mu\text{s}$  and the baseline as the average of hits from 0.5s before the onset to the onset, we integrate the number of hits over 11 s starting from 1 s before the onset. The baseline is 1.214 hits per hardware counter and composed of dark noise of PMTs and decay of radioisotopes from the wall [5]. Table 3 summarizes the results. The total number of hits recorded by the SN module with and without the veto module is almost the same, showing a difference of about 2%. However, the QBEE recorded  $2.266 \times 10^9$  hits without the Veto module and  $1.944 \times 10^9$  hits with the Veto module. Indeed, the QBEE loses about 30% of PMT hits due to buffer overflows for a burst with 30 million events, but 40% of hits are vetoed Veto module. Though more events are seemingly lost due to the veto, we cannot use the remaining 70% hits without Veto module for physics analyses as described in Section 5. However, the hits remaining after vetoing the QBEE can still be used.

	QBEE	SN module
Veto module <b>off</b>	$2.266 \times 10^9$	$3.392 \times 10^9$
Veto module <b>on</b>	$1.944 \times 10^9$	$3.318 \times 10^9$

**Table 3** Summary of the total number of hits recorded by each module during LD testing.

## 5 Burst analysis demonstration

During the LD tests described above, each flash of the LD is meant to correspond to a neutrino event from a nearby supernova. In this section we analyze LD test data to reconstruct the simulated supernova timing structure. Figure 11 shows PMT hits from the tail of an LD test with a total of 30 million flashes. During the tail phase the flash rate is about 1.1 MHz, resulting in roughly 90 flashes during the  $60 \mu\text{s}$  time window assigned to events in SK. Typically only one event per such time window is expected during normal operations and pile-up of this sort is not considered in ordinary SK analyses.

Here LD burst data are separated by the hardware counter and the number of flashes during each counter is calculated by counting the number of PMT hits in a  $68.25 \mu\text{s}$  time window. Clusters of hits above a threshold, 25, are considered to be a flash. When this threshold is less than 21 hits, LD flashes cannot be separated from random dark noise in the detector. Similarly, when the threshold is higher than 29 true LD flashes start to be rejected. The number of flashes expected during vetoed hardware counters is calculated by interpolating based on the reconstructed flash rate in the previous hardware counter. Figure 12 shows the reconstructed LD burst and Figure 13 shows the same data zoomed in around the 1.38 s period. The black dots are the real data taken by the QBEE and red dots show interpolated flashes from the previous data.

Summing the reconstructed flashes in Figure 12 from 0 to 10 s results in a total of 28.8M flashes. This value is close to the 30 million flashes expected. The difference is due to pile-up of the flashes themselves during the highest flash rate of 0.5 s. Such pile-up events are reconstructed as a signal flash with the procedure above. Additionally, the expected number of flashes is based on the number of pulses sent to the LD. It is possible that the LD did not flash during the highest event rates, so the number of reconstructed flashes may be closer to the truth than the number 30 million is. For example, the number of clocks to the LD is 29.9M. On the other hand, the number of counts recorded by the monitor PMT in Figure 5 is 28.6M events.

While analyses like the above are simple, we can nonetheless obtain physics information from them. Knowing the relationship between the number of hit PMTs and the deposited

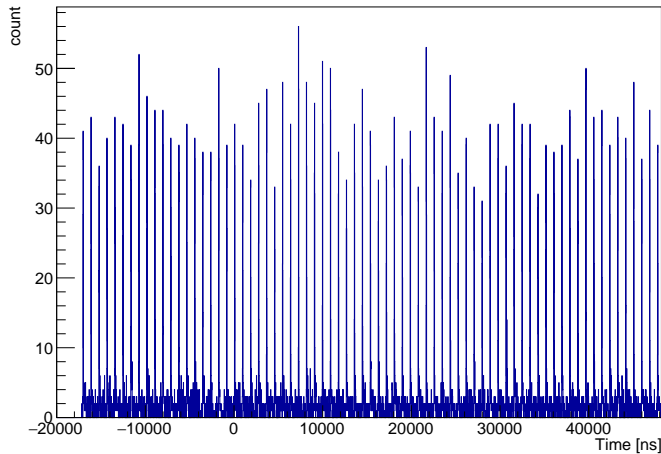


**Fig. 11** LD flashes in the tail of an event time window. Each peak corresponds to an LD flash. The horizontal axis is time in nanoseconds and the vertical axis is the number of PMT hit counts per 16 ns.

energy from calibrations, the neutrino flux during the SN burst can be estimated without detailed time and charge information from the PMTs. When the QBEEs are not vetoed, they provided detailed event information as seen in Figure 11, such that if we assume the time evolution of the SN does not change much during the veto periods the neutrino flux therein can also be estimated by extrapolation from the surrounding QBEE data. Since the most rapid supernovae flux evolution is much longer than the typical veto length, milliseconds [9, 14, 15]) compared to tens of microseconds, this extrapolation should be robust.

## 6 Long-term Testing

As the Veto module is a critical component of SK’s ability to observe even the highest event rate supernovae, it must operate continuously and without interfering with normal DAQ operations. For this reason we conducted a year-long test of the module without allowing it to veto the normal DAQ even when the module was triggered. Data from the long-term Veto module test was collected from July 2021 to June 2022. Using recorded information of the veto signal (“storage” in Figure 3), times were matched with events from the standard DAQ to identify what types of events triggered the Veto module. The event type is determined using the SK event display and Time-Charge histograms like that in Figure 14.

We observed two types of events which trigger the Veto module: highly energetic muons and PMT-generated flashers. Cosmic ray muons enter the tank at approximately 2 Hz and

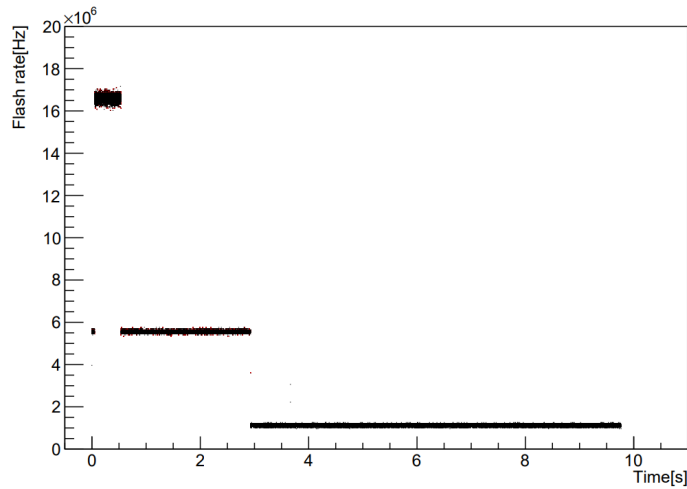


**Fig. 12** Flash rate of the LD test with 30 million events. The horizontal axis is time in seconds and the time origin is the same as in Figure 9. The vertical axis is the number of LD flashes per second.

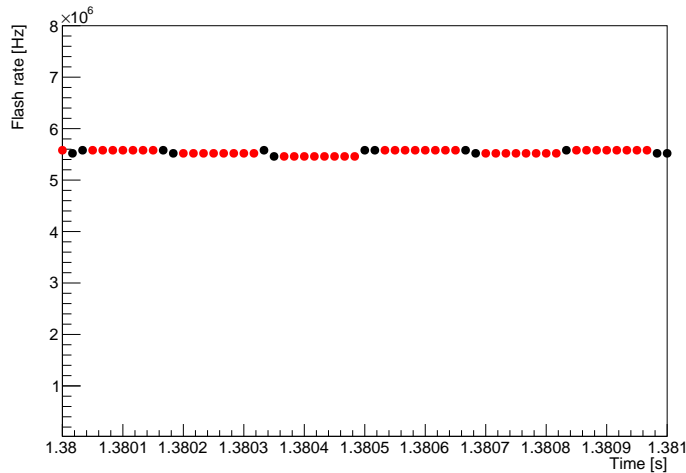


**Fig. 13** Zoom in of the area around 1.38 s of Figure 12. The black points are data from the QBEE and red points are extrapolated points based on the preceding black points.

some deposit enough energy to both saturate the PMTs and generate secondary particles through radiative losses. This may cause both a large number of hit PMTs in a short period of time as well as a significant amount of delayed hits from afterpulsing, which can result in satisfying the conditions to trigger the Veto module. PMT-generated flashers, on the other hand, are a phenomenon that occurs when a PMT emits a strong flash due to a discharge

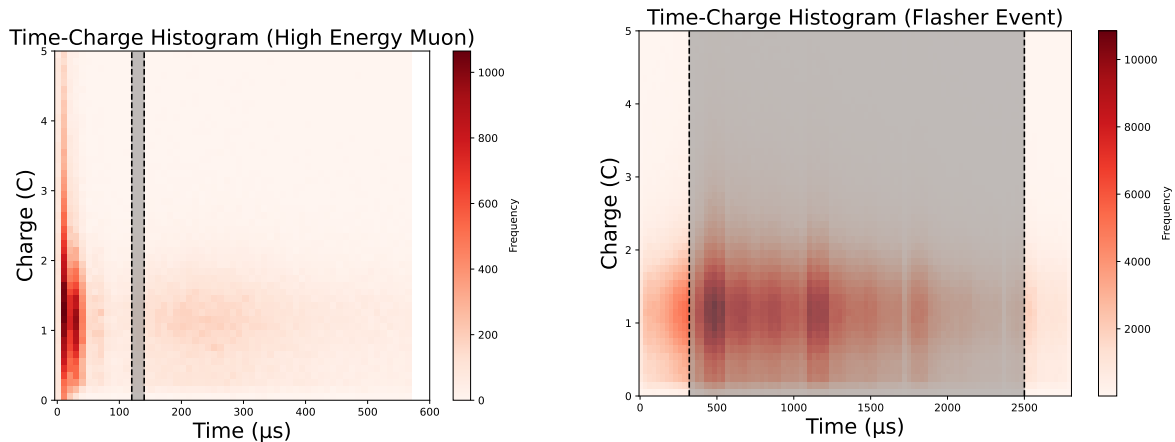


**Fig. 14** Time-Charge histogram of hit PMTs from a high energy muon event (left) and from a flashing PMT (right). Gray bands indicate periods where the vetos were issued. The muon event has a delayed veto signal of approximately  $200 \mu s$  due to inherent DAQ module latency.

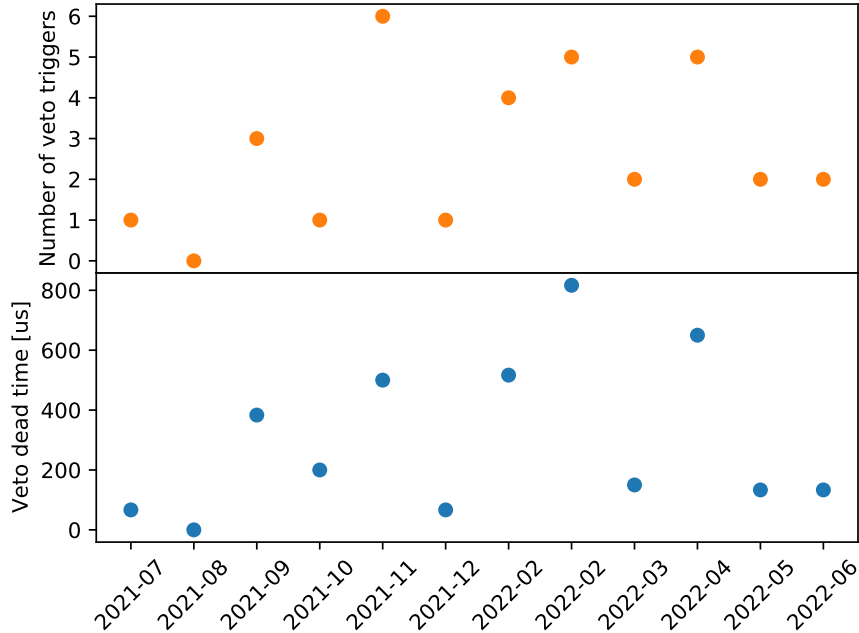
inside the PMT or the voltage divider. Repeated flashing of this sort, together with events produced by the reflections of those flashes can also mimic the event rate expected for a nearby supernova.

Figure 15 shows histograms of the number of triggered Veto module and the veto dead-time from July 2021 to June 2022. We found that the Veto module triggered 33 times during the long-term test, resulting in  $3616 \mu s$  of veto dead-time. Looking at the Charge-Time profiles of those events, 30 are classified as highly energetic muons and one event is identified as a PMT-generated flasher. The left panel of Figure 14 shows the profile of highly energetic muon whose event length is  $50 \mu s$ , The right panel shows the PMT-generated flasher which continues for  $2500 \mu s$  and produces three bands of activity with a period of  $600 \mu s$ . These periodic bands are characteristic of PMT-generated flashers.

Based on this test we expect roughly three vetos per month with an average deadtime per event of  $100 \mu s$ . Over the course of a full year approximately three milliseconds of data will be lost to vetos, which is negligible compared to the detector livetime.

## 7 Analysis of veto dead-time using Monte Carlo simulations

Though we proved in previous sections that Veto module can prevent the QBEE from overflowing, allowing SK to take quality data during high event rate periods, the Veto module itself also creates some dead time via its vetoes. We have developed a new Monte Carlo



**Fig. 15** Triggering frequency of the Veto module together with the dead-time incurred during physics runs due to those vetos taken from July 2021 to June 2022. The top panel is the number of triggered Veto modules and the bottom panel is the dead-time.

(MC) simulation to investigate how much data will be vetoed by the module in response to supernovae simulated at various distances from the Earth.

### 7.1 Method

Since 2020 Super-Kamiokande has been loaded with gadolinium sulphate (0.01% in 2020 and 0.03% in 2022) and operated as SK-Gd [16]. The purpose of the Gd loading is to enhance neutron detection and to thereby help separate inverse beta decay (IBD) events,  $\bar{\nu}_e + p \rightarrow e^+ + n$ , from other reactions. In water Cherenkov detectors IBD is the dominant interaction mode expected from supernovae, accounting for 90% of the observed neutrinos. When neutrons are captured on gadolinium nuclei, a cascade of multiple gamma rays with 8 MeV of energy in total are emitted. While this makes the neutron capture easy to identify it creates additional, delayed PMT hit activity that is likely to affect the Veto module's operation.

In our simulation studies we therefore consider both a pure water target and a gadolinium-loaded-water target. The process includes inputting the supernova model, supernova distance

and coordinates, and MSW neutrino oscillation assumptions [17] into the SK event vector generator for supernova simulations called SKSNSim (Super-Kamiokande Supernova Simulation).

The software generates neutrino events according to input cross sections for IBD, charged-current interactions on oxygen, and neutral current interactions on oxygen convolved with the flux expected from the chosen supernova model. Output from SKSNSim is passed to the Geant4-based SK detector simulation, SKG4 (Super-Kamiokande Geant4) [18], which simulates the passage of the outgoing particles through the detector. It simulates the passage of Cherenkov radiation through water (or the Gd solution [19, 20]), including photon scattering, absorption, and reflection, and simulates the PMT and electronic responses [21]. All analyses using Gd-loaded water in this study assume a 0.03% Gd concentration [16]. Afterwards realistic dark noise taken from random trigger data from SK is added to the output of the detector simulation. These simulated events are then analyzed to reconstruct the number of SN triggers and to determine when and for how long the Veto module would issue vetos.

## 7.2 *Supernova Models*

Due to the expensive computational resources required for supernova burst simulations, supernova models typically only simulate up to about 1 second after the bounce in multi-dimensional calculations. To overcome computational resource constraints, simplified assumptions and approximations (e.g., one-dimensional methods in a spherically symmetric geometry) are necessary for simulating neutrino emissions over long times. This study chooses two long-term one-dimensional supernova models: the Nakazato model [15] and the Mori model [9]. Both models have flux predictions reaching up to 20 s after the core bounce. An important distinction is that the luminosity of neutrinos predicted by the Nakazato model is higher than that of the Mori model. Consequently, we expect the veto dead-time generated by the Nakazato model to be longer than that of the Mori model. When simulating supernovae from these models, we select distances ranging from 100 pc to 1 kpc at intervals of 100 pc.

## 7.3 *Results and Discussion*

Figure 16 shows the number of PMT hits per  $17.1 \mu\text{s}$  recorded through one SN module for a simulated supernova located at 800 pc from the earth as described by the Nakazato model. The distribution peaks between 0.03 s and 0.2 s hits during which the SN trigger condition of more than 100 hits continuing for  $68.3 \mu\text{s}$  or more is satisfied. Figure 17 then shows the issued SN triggers for the same supernova for the region from 0.443 s to 0.447 s.



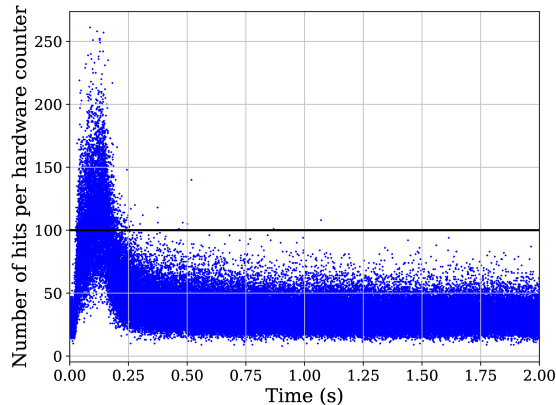


**Fig. 16** Hits per a hardware counter as measured by the SN module for a supernova burst at a distance of 800 pc from the Earth assuming the Nakazato model. The horizontal axis is the time measured from the first hit. The peak area meets the trigger condition of the SN module.

In this window and there are SN triggers which meet the condition of Veto module around 0.445 s shown in Table 2, and during which the QBEEs would be vetoed by the Veto module.

In this way, the amount of dead-time incurred by supernovae as a function of distance is calculated and summarized in Figure 18. The simulation results show that supernovae begin to trigger the Veto module at distances between 700 pc and 850 pc. For SK-Gd the module is triggered by more distant supernovae than pure water due to the gamma rays emitted when neutrons are captured by Gd. The Gd doping increases the total veto dead-time by approximately a factor of 1.6 regardless of the supernova’s distance. Comparing the Nakazato and Mori models, we find that the distance at which the Nakazato model triggers Veto module is closer than that for the Mori model, as expected by the higher luminosity in the former. Table 4 summarizes the distances at which veto signals start being issued. With a 0.011% concentration of Gd, this distance is closer by 20-30 pc and the start of the Nakazato model is closer by 100 pc than that of the Mori model.

## 8 Summary

This paper describes new DAQ modules introduced at SK to insure the as much data as possible from a nearby supernova is recorded without overflowing or crashing the standard QBEE-based DAQ. These modules, the SN module and Veto module, effectively prescale

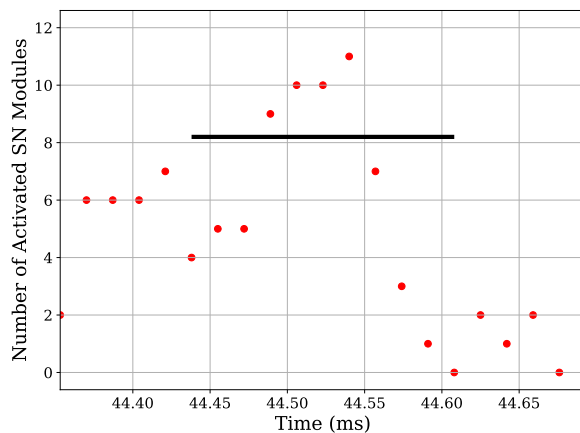


**Fig. 17** SN triggers for the 800 pc supernova of the Nakazato model. The Veto module conditions are listed in Table 2. The horizontal axis is an expansion of the 0.4435 s to 0.447 s period in Figure 16.

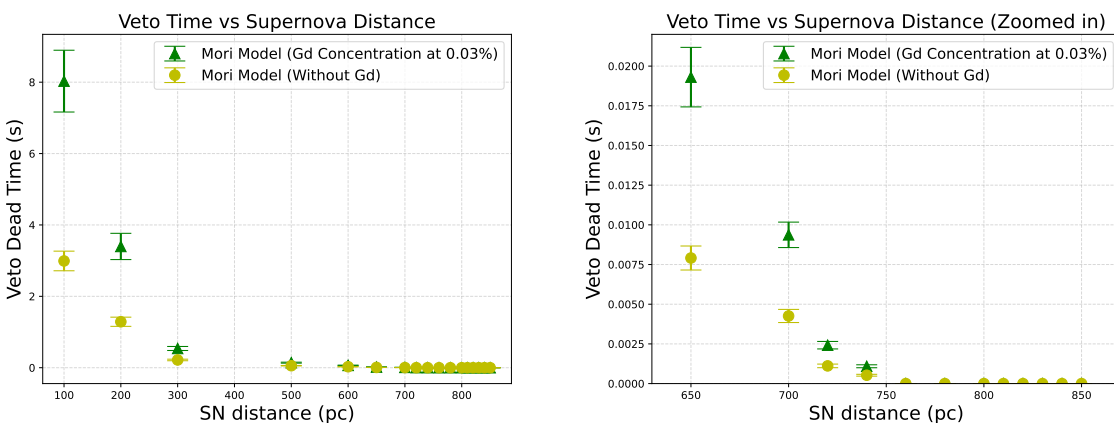


**Fig. 18** Dead time incurred by vetoes issued by the Veto module as a function of simulated supernova distance. Results from the entire survey of distances, from 100 pc to 1000 pc, are shown in the left panels, and enlarged views of distances between 550 pc and 900 pc are shown in the right panels. The error bars show  $1\sigma$  statistical uncertainties. It should be noted that 170 pc is the distance between Betelgeuse and Earth.

PMT hits, vetoing the standard DAQ activity during periods with very high event rates to prevent buffer overflows.

The performance of these modules was checked with dedicated high-event-rate laser diode data taking and confirmed that the SN module takes dead-time free data and the Veto module prevents the QBEEs from overflowing. Further, an analysis of those data was successfully

Supernova models	Waters	Start distances (pc)
Nakazato	0.03% Gd	850 – 900
Nakazato	pure water	820 – 830
Mori	0.03% Gd	730 – 740
Mori	pure water	710 – 720

**Table 4** Distances at which the Veto module starts being triggered for the Nazakato and Mori models assuming the pure water SK and SK-Gd configurations.

able to reconstruct the input number of diode flashes, indicating the robustness of the data taking during high rate scenarios. Long-term testing of the modules from June 2021 to May 2022 confirmed that the modules do not affect ordinary operations at SK and identified two types of events that trigger the Veto modules: energetic cosmic ray muons and flashing PMTs. However, even with those triggers less than 1 ms of deadtime is expected per year with the new modules.

Simulations were performed to understand the behavior of the modules in response to nearby supernovae using two different supernova models and assuming both pure and Gd-loaded detector conditions. Under all conditions we find that the modules will be triggered for a supernova located at or closer than 800 pc. For Betelgeuse, which is at 170 pc away from the earth, the veto dead-time is found to be between 3 s to 4 s. In spite of this dead-time, the Veto module and SN module will allow us to nonetheless analyze the bulk of the supernova neutrino emission from Betelgeuse, which should continue for more than 1 minute.

## Acknowledgements

We gratefully acknowledge the cooperation of the Kamioka Mining and Smelting Company. The Super-Kamiokande experiment has been built and operated from funding by the Japanese Ministry of Education, Culture, Sports, Science and Technology, the U.S. Department of Energy, and the U.S. National Science Foundation. Some of us have been supported by funds from the National Research Foundation of Korea (NRF-2009-0083526 and NRF 2022R1A5A1030700) funded by the Ministry of Science, Information and Communication Technology (ICT), the Institute for Basic Science (IBS-R016-Y2), and the Ministry of Education (2018R1D1A1B07049158, 2021R1I1A1A01042256, the Japan Society for the Promotion of Science, the National Natural Science Foundation of China under Grants No.11620101004,

the Spanish Ministry of Science, Universities and Innovation (grant PGC2018-099388-B-I00), the Natural Sciences and Engineering Research Council (NSERC) of Canada, the Scinet and Westgrid consortia of Compute Canada, the National Science Centre (UMO-2018/30/E/ST2/00441) and the Ministry of Education and Science (DIR/WK/2017/05), Poland, the Science and Technology Facilities Council (STFC) and Grid for Particle Physics (GridPP), UK, the European Union’s Horizon 2020 Research and Innovation Programme under the Marie Skłodowska-Curie grant agreement no.754496, H2020-MSCA-RISE-2018 JENNIFER2 grant agreement no.822070, and H2020-MSCA-RISE-2019 SK2HK grant agreement no. 872549.

## References

- [1] K. Sato and H. Suzuki, *Physics Letters B*, **196**(3), 267–271 (1987).
- [2] A. Burrows, *Astrophys. J.*, **334**, 891 (1988).
- [3] James M. Lattimer and A. Yahil, *The Astrophysical Journal*, **340**, 426 (1989).
- [4] Y. Fukuda et al., *Nucl. Instrum. Meth. A*, **501**, 418–462 (2003).
- [5] M. Mori et al., *Astrophys. J.*, **938**(1), 35 (2022), arXiv:2206.01380.
- [6] K. Hirata et al., *Phys. Rev. Lett.*, **58**, 1490–1493 (1987).
- [7] R.M. Bionta et al., *Phys. Rev. Lett.*, **58**, 1494 (1987).
- [8] E. N. Alexeyev et al., *Physics Letters B*, **205**(2-3), 209–214 (1988).
- [9] M. Mori et al., *Progress of Theoretical and Experimental Physics*, **2021**(2), 023E01 (2021), arXiv:2010.16254.
- [10] M. Joyce et al., *Astrophys. J.*, **902**(1), 63 (2020), arXiv:2006.09837.
- [11] H. Nishino et al., *Nucl. Instrum. Meth. A*, **610**, 710–717 (2009), arXiv:0911.0986.
- [12] Y. Arai, *Nucl. Instrum. Meth. A*, **453**, 365–371 (2000).
- [13] A. Orii et al., Development of new data acquisition system at Super-Kamiokande for nearby supernova bursts, In *2014 IEEE Nuclear Science Symposium and Medical Imaging Conference and 21st Symposium on Room-Temperature Semiconductor X-ray and Gamma-ray Detectors* (2016).
- [14] T. Takiwaki et al., *Astrophys. J.*, **786**(2), 83 (2014), arXiv:1308.5755.
- [15] K. Nakazato et al., *The Astrophysical Journal Supplement Series*, **205**(1), 2 (2013).
- [16] K. Abe et al., *Nucl. Instrum. Meth. A*, **1027**, 166248 (2022), arXiv:2109.00360.
- [17] Amol S. Dighe et al., **62**(3), 033007 (2000).
- [18] Masayuki Harada, Geant4 based simulation study for super-kamiokande, In *Journal of Physics: Conference Series*, volume 1468, page 012255. IOP Publishing (2020).
- [19] K. Hagiwara et al., *Progress of Theoretical and Experimental Physics*, **2019**(2), 023D01 (2019), <https://academic.oup.com/ptep/article-pdf/2019/2/023D01/27970473/ptz002.pdf>.
- [20] T. Tanaka et al., *Progress of Theoretical and Experimental Physics*, **2020**(4), 043D02 (2020), <https://academic.oup.com/ptep/article-pdf/2020/4/043D02/33040537/ptaa015.pdf>.
- [21] H. Nishino et al., **1**, 127–132 (2007).